

UNIVERSITY OF  
CALIFORNIA

*Radiation  
Laboratory*

TWO-WEEK LOAN COPY

*This is a Library Circulating Copy  
which may be borrowed for two weeks.  
For a personal retention copy, call  
Tech. Info. Division, Ext. 5545*

BERKELEY, CALIFORNIA

## **DISCLAIMER**

This document was prepared as an account of work sponsored by the United States Government. While this document is believed to contain correct information, neither the United States Government nor any agency thereof, nor the Regents of the University of California, nor any of their employees, makes any warranty, express or implied, or assumes any legal responsibility for the accuracy, completeness, or usefulness of any information, apparatus, product, or process disclosed, or represents that its use would not infringe privately owned rights. Reference herein to any specific commercial product, process, or service by its trade name, trademark, manufacturer, or otherwise, does not necessarily constitute or imply its endorsement, recommendation, or favoring by the United States Government or any agency thereof, or the Regents of the University of California. The views and opinions of authors expressed herein do not necessarily state or reflect those of the United States Government or any agency thereof or the Regents of the University of California.

## CROSS SECTIONS OF ANTIPROTONS IN HYDROGEN, BERYLLIUM, CARBON, AND LEAD

Bruce Cork, Glen R. Lambertson,  
Oreste Piccioni,<sup>\*</sup> and William A. Weasel

Radiation Laboratory  
University of California  
Berkeley, California

February 1, 1957

### I. INTRODUCTION

Previous experiments have shown that the antiproton interacts strongly with matter.<sup>1, 2, 3, 4</sup> At 500 Mev for lead glass, copper, and beryllium, and at lower energies for photographic emulsions, the absorption cross section is significantly greater than geometric. The purpose of the experiment reported here was to extend to other elements the measurements on the interaction of antiprotons and, in particular, to measure as a function of energy the total proton-antiproton cross section, which is of central importance to the understanding of the nucleon-antinucleon interaction.

In order to fit the experimental program into a feasible time schedule, considerable effort was spent in the development of a usable antiproton beam of high intensity. The use of this beam in the production and identification of antineutrons has been described in an earlier report.<sup>5</sup>

The magnetic channel and the basic electronics are described in Sections II and III respectively, while operation of the antiproton identification scheme is included in Section IV. The attenuation experiment in hydrogen is described in Section V; and the measurements on beryllium, carbon, and lead in Section VI.

### II. MAGNETIC BEAM CHANNEL

Antiprotons were produced in a 6-inch-long beryllium target in the internal beam of the Bevatron (Fig. 1). From this point at  $5^\circ$  from the end of the quadrant, negative particles produced in the forward direction were deflected by the magnetic field toward a thin (3/16-inch) section of the vacuum-tank wall.

<sup>\*</sup>On leave from Brookhaven National Laboratory.

The external beam channel (Fig. 1) was designed to carry a beam of considerable momentum width over the required time-of-flight path. Five quadrupole lenses of nominally 4-inch aperture were employed; each lens was composed of two quadrupoles 8 inches long and one 16 inches long. The first lens,  $Q_1$ , was placed as close as feasible (130 inches) to the internal target so as to obtain the maximum solid angle of acceptance. To attain sufficient focusing power from available units and to allow some choice in magnification, the three quadrupoles in  $Q_1$  were arranged to function as a two-element lens. The two 8-inch units were adjacent with their fields aiding and in a direction opposite to that in the 16-inch quadrupole that followed; a 7.25-inch interval between these quadrupoles was the minimum allowed by the water and electrical connections.  $Q_1$  formed an image of the beryllium target at the entrance to  $Q_2$  and effected a transition into the repeating pattern of lenses that followed. Each of the four lenses after  $Q_1$  was adjusted to focus particles emerging from the lens preceding it into the aperture of the succeeding lens. For particles at the center of the momentum interval accepted, lenses  $Q_2$  and  $Q_4$  were located at the target image points, and in this sense bear some analogy to field lenses in an optical system. Such an array of lenses uniformly spaced at twice the focal length presents a good aperture to particles from an extended source and over a broad momentum range; it is a feature of this system that the aperture remains large when the channel is lengthened by the addition of lenses. The broad admittance of this beam channel not only permitted a large flux of particles, but also reduced beam loss from scattering in the vacuum-tank wall and in the scintillators. Our lenses  $Q_2$  through  $Q_5$  were each symmetric arrangements of quadrupoles with the 16-inch unit in the center separated from the 8-inch units by 10.5-inch intervals. The series of magnetic lenses carried negative particles a distance of about 100 feet from the target. At 1.4 Bev/c momentum, the lenses after  $Q_1$  operated with gradients of about 3600 gauss/inch;  $Q_1$  had about 2800 gauss/inch, and the lenses were spaced with 251 inches between centers.

The dispersion of the magnetic field in the Bevatron produced a horizontal extension of the target image at  $Q_2$ . The magnification of  $Q_1$  and deflection in the first analyzer magnet,  $A_1$ , increased this effect and allowed adjustment of the momentum interval entering the aperture of  $Q_2$ . The analyzer magnets also served to reject positive particles that scattered into or were produced along the beam path.

In addition, three monitors were provided. A scintillation telescope  $M_1$ , looking directly at the internal target, monitored the beam spill-out. A coincidence circuit  $M_2$ , connected to alternate outputs of Counters C and E and timed to count  $w$  mesons, monitored the channel flux; and the signal from a beam induction electrode in the Bevatron was integrated to provide a record of the total circulating beam.

The structure of the Bevatron circulating beam during acceleration has pronounced rf modulation. To reduce the peak counting rate encountered by our time-of-flight scintillators, the following beam spill-out technique was employed. The circulating proton beam was steered into a thin aluminum foil (.0003 inch) at the outer radius. The energy loss sustained in repeated passage through this foil caused the protons to become phase-unstable and to spiral inward in the increasing magnetic field of the Bevatron. In the several milliseconds required to spiral into the beryllium target all phase coherence was lost, and a beam spill-out of uniform intensity was obtained. By control of the rate at which the initial beam was driven into the foil, the length of the spill-out could be adjusted. In this experiment, a 100-millisecond spill was used, corresponding to an energy range of the internal beam of from 5.8 to 6.2 Bev.

#### IV. IDENTIFICATION OF ANTIPROTONS

The intervals AC, CE, BD, and DF between counters were each long enough to reject single  $w$  mesons by a large factor ( $\approx 10^3$ ) when the counters were timed for antiprotons ( $\beta \approx 0.625$  to  $0.83$ ). Similarly, twofold accidentals were rejected because, for example, two mesons that simulated an antiproton in the interval AC could not simultaneously do so in the interval CE. The use of two such coincidence circuits serves a double purpose. First, the probability that an accidental coincidence occurs in two slightly detuned independent circuits is the product of the probabilities for each. Thus the rejection of mesons is improved. In addition, some rejection against threefold accidentals can be obtained by staggering the intervals so that we have  $AC > CE$  while  $BD < DF$ . Separation of the antiprotons was, of course, most difficult at the highest velocity employed ( $\beta = 0.83$ ). The lengths of the cables connecting each counter with the coincidence circuit determined the velocity to which the electronic system was sensitive, and therefore defined the mass of particles selected. Figure 3 shows the number of coincidences obtained at 1.4 Bev/c as the relative





On the other hand, events that are not detected in L are principally inelastic, as is indicated by the broad lower spectrum of Fig. 8. The peak in this spectrum is attributed to antiprotons that scatter elastically at angles large enough to miss counter L.

Figure 9 shows a similar spectrum obtained for 1959 antiprotons incident upon X with L placed in "poor" geometry ( $\theta_1/2 = 25^\circ$ ). The broad background of the upper spectrum of Fig. 9 indicates that relatively more secondaries are detected by L, and the absence of a peak in the lower spectrum indicates that elastically scattered antiprotons are contained within L.

From the spectra of Fig. 8 we have determined the total carbon-antiproton cross section. Results of the cross-section measurements for hydrogen described in Section V have been used to correct the observed transmission of toluene ( $C_7H_8$ ) to obtain the transmission for pure carbon.

From the spectra of Fig. 9 we have determined the inelastic carbon-antiproton cross section. Correction for hydrogen absorption has been made with the assumption that the proton-antiproton cross section is three-fourths inelastic. The justification for this is that, as will be seen, the inelastic antiproton cross section for carbon, and probably for beryllium, is considerably larger than the elastic. Since the total correction for hydrogen absorption amounts to only 15% of the carbon-antiproton cross section, the uncertainty introduced by this assumption is small.

The forward-scattering correction to the total cross-section measurement has been made, as for the beryllium measurements, by assuming that the region of interaction is an absorptive disk. The correction, although rather large, is relatively independent of the assumed radius of interaction. The value for the corrected total cross section  $\sigma_{T_{cor}}$  given in Table III, is obtained for that radius which gives a computed value for the inelastic cross section equal to the measured value. The table includes as well the results of similar measurements at 0.9 Bev/c.  $T_p$  is the kinetic energy of the antiproton at the center of the carbon (toluene) target and is uncertain by  $\pm 5\%$ . The expressed uncertainties in the cross sections are statistical only.

### C. Lead

The desirability of extending the measurement of antiproton cross sections to elements other than carbon suggested the use of wafer inserts in the toluene scintillator. This might be especially helpful for heavy elements, for which the performance of good-geometry attenuation experiments is





### ACKNOWLEDGMENTS

We take this opportunity to thank Dr. Edward J. Lofgren and the Bevatron operating staff for their invaluable cooperation. The help of Laurence S. Beller, Charles A. Coombes, Fred H. G. Lothrop, and Douglas Parmentier during the experiment is greatly appreciated. The liquid hydrogen target was designed by William M. Salsig and Garth E. Cook. Marion J. Jones was responsible for the design and operation of the numerous magnet power supplies. A group working with Felix C. Caldera built much of the electronics.

This work was done under the auspices of the U. S. Atomic Energy Commission.

## REFERENCES

1. Brabant, Cork, Horwitz, Moyer, Murray, Wallace, and Wenzel, *Phys. Rev.* 101, 498 (1956), and *Phys. Rev.* 102, 1622 - 1626 (1956).
2. Chamberlain, Keller, Segrè, Steiner, Wiegand, and Ypsilantis, *Phys. Rev.* 102, 1637 (1956).
3. Chamberlain, Chupp, Ekspong, Goldhaber, Goldhaber, Lofgren, Segrè, Wiegand, Amaldi, Baroni, Castagnoli, Franzinetti, and Manfredini, *Phys. Rev.* 102, 921 (1956).
4. Barkas, Birge, Chupp, Ekspong, Goldhaber, Goldhaber, Heckman, Perkins, Sandweiss, Segrè, Smith, Stork, Van Rossum, Amaldi, Baroni, Castagnoli, Franzinetti, and Manfredini, *The Antiproton-Nucleon Annihilation Process*, University of California Radiation Laboratory, Report No. UCRL-3520, Sept. 1956.
5. Cork, Lambertson, Piccioni, Wenzel, *Phys. Rev.* 104, 1193 (1956).
6. Chamberlain, Chupp, Goldhaber, Segrè, Wiegand, Amaldi, Baroni, Castagnoli, Franzinetti, and Manfredini, *Il Nuovo Cimento, Serie X*, Vol. 3, 447 (1956).
7. H. A. Bethe and F. de Hoffman, "Mesons and Fields", Vol. II, pg. 76, Row, Peterson and Company, New York, 1950.
8. Wright, Powell, Maenchen, and Fowler, *Bulletin of the A. P. S., Series II*, Vol. I, pg. 376 (1956).
9. Cork, Wenzel, and Causey, *Bulletin of the A. P. S., Series II*, Vol. I, pg. 376 (1956).
10. Chen, Leavitt, and Shapiro, *Phys. Rev.* 103, 211 (1956).
11. H. Duerr and E. Teller, *Phys. Rev.* 101, 494(L) (1956).
12. H. Duerr, *Phys. Rev.* 103, 469 (1956).
13. Chen, Leavitt, and Shapiro, *Phys. Rev.* 99, 657 (1955).

## FIGURE CAPTIONS

- Fig. 1. Antiproton selecting system.  $Q_1$  through  $Q_5$  are three-element quadrupole lenses and  $A_1$  and  $A_2$  are beam-deflecting magnets. A through F are plastic scintillation counters.
- Fig. 2. Block diagram of basic electronics. A through L are scintillation counters;  $C_1$  through  $C_8$  are coincidence circuits;  $D_1$  through  $D_4$  are discriminators.  $M_1$  and  $M_2$  are monitors of the internal target and the magnetic channel flux, respectively. Amplifiers are not shown.
- Fig. 3. Delay curve of time-of-flight selector at 1.4 Bev/c. Calculated delays for  $\pi^-$  mesons,  $K^-$  mesons, and antiprotons are shown on the horizontal axis. Coincidence  $C_1C_2$  is made between the outputs of the two threefold coincidence circuits.
- Fig. 4. Diagram of liquid hydrogen target construction.
- Fig. 5. Layout of attenuation experiment with hydrogen target.
- Fig. 6. Total antiproton-proton cross-section results. Uncertainties given are statistical only. Cross sections for p-p and p-n interactions are shown for comparison.
- Fig. 7. Liquid scintillator target assembly. The dashed outlines indicate the location, when in place, of water inserts of target material.
- Fig. 8. Pulse-height spectra in X for incident 1.4-Bev/c antiprotons. The 330 events are separated according to whether or not a coincident count occurred in a scintillator, L, which subtended at X an angular half width of  $2.65^\circ$ .
- Fig. 9. Pulse-height spectra in X for incident 1.4-Bev/c antiprotons. These 1959 events are also separated as in Fig. 8, but with L subtending a half angle of  $25^\circ$  in this case.

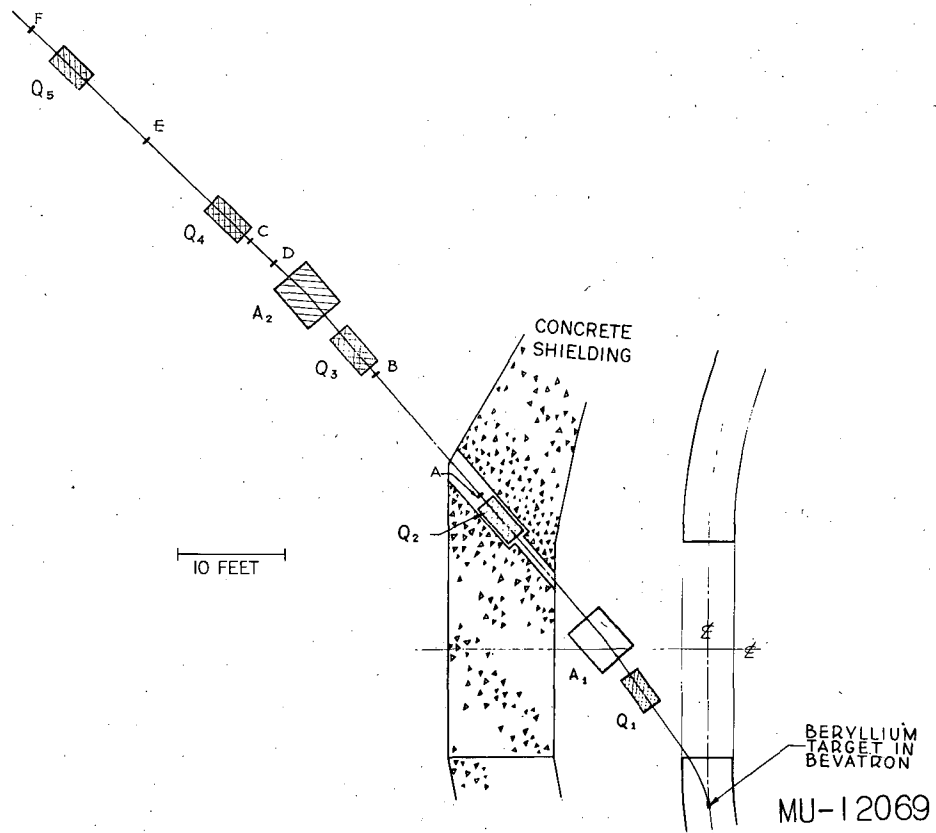
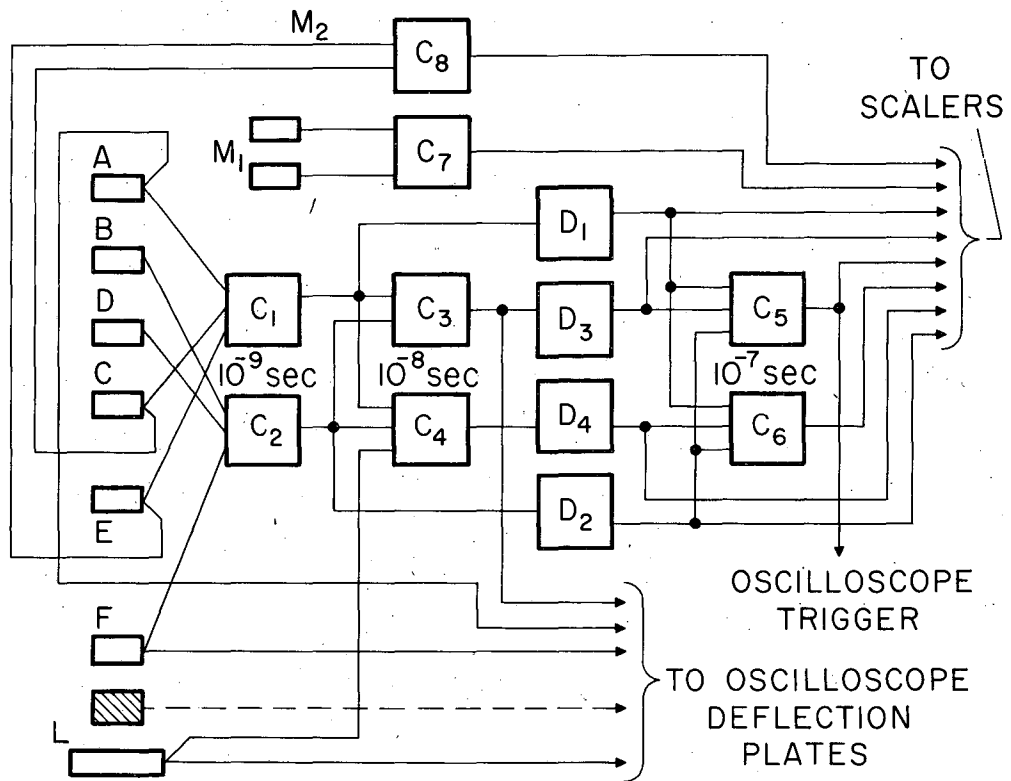
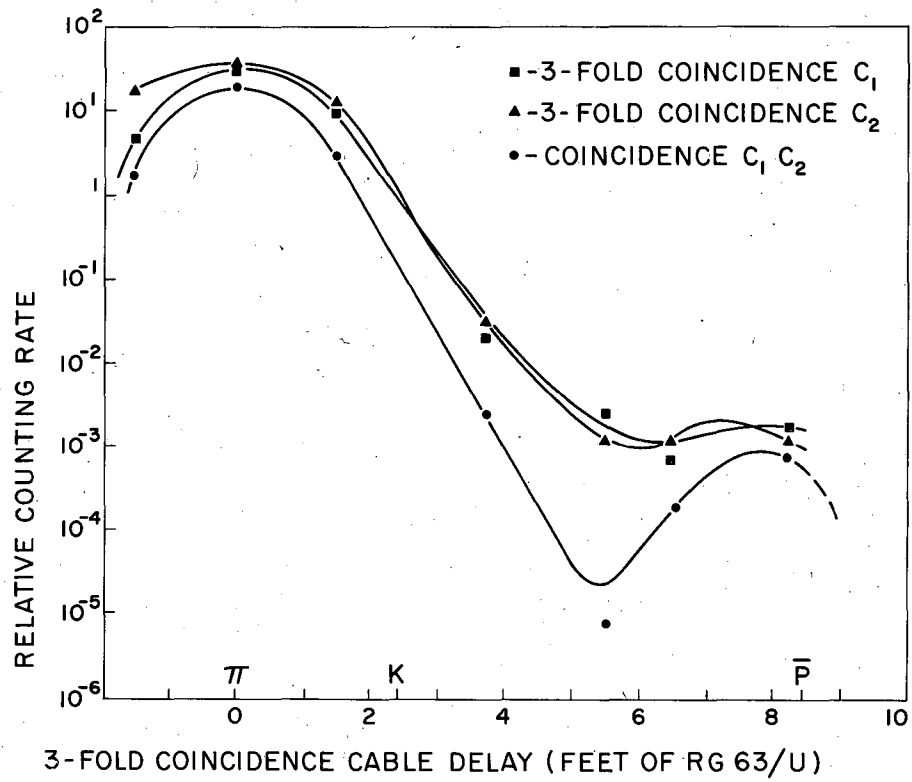


Fig. 1



WU-12524

Fig. 2



MU-12838

Fig. 3

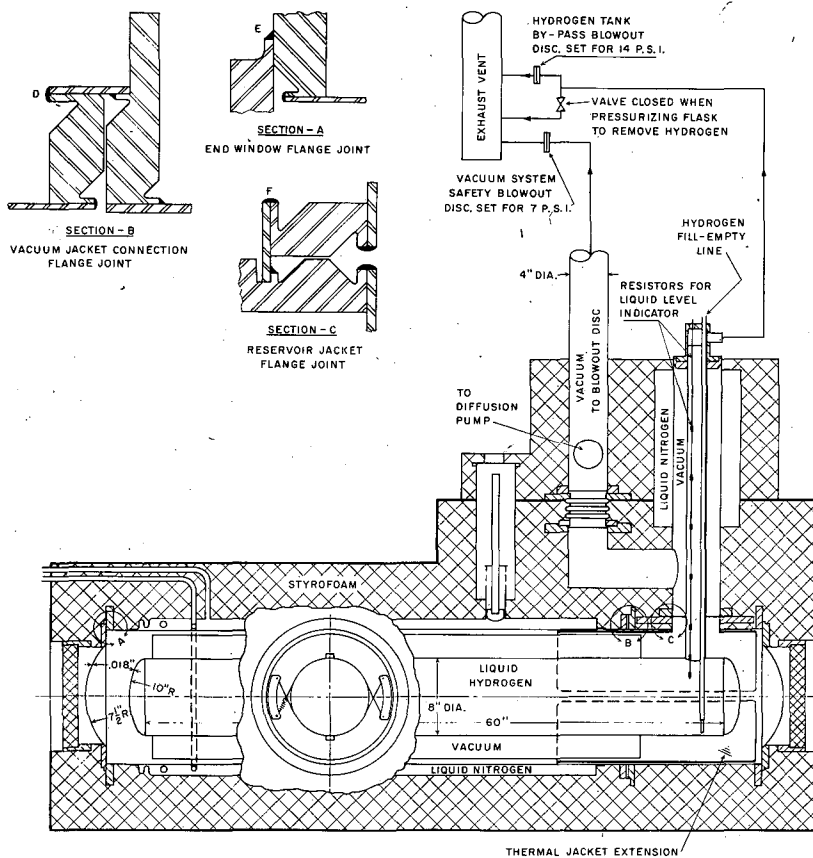
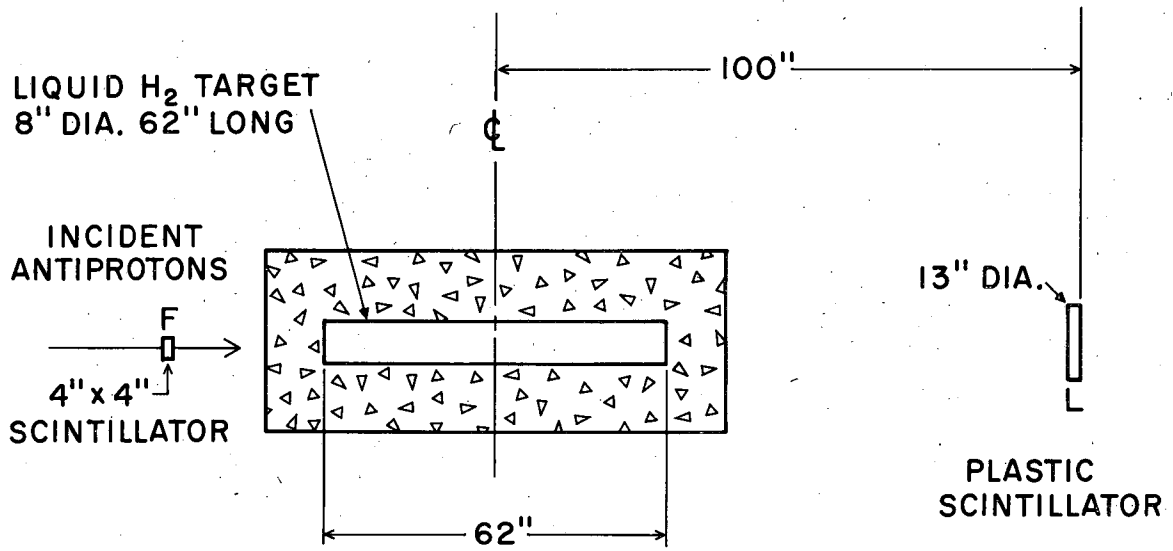


Fig. 4



MU-12836

Fig. 5

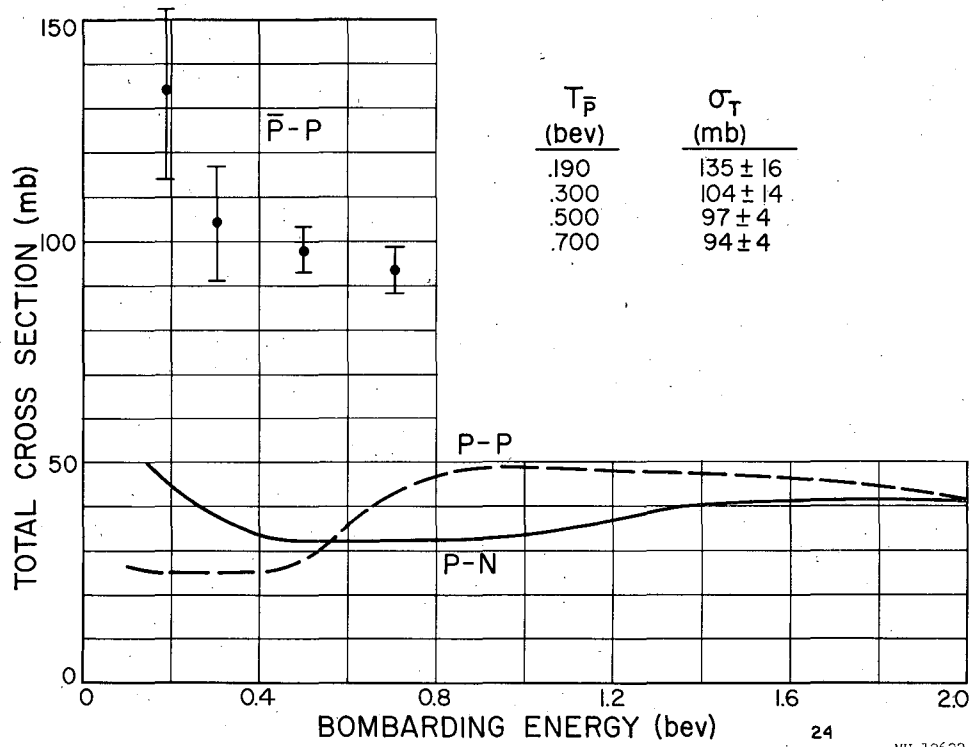
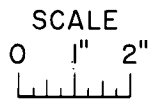
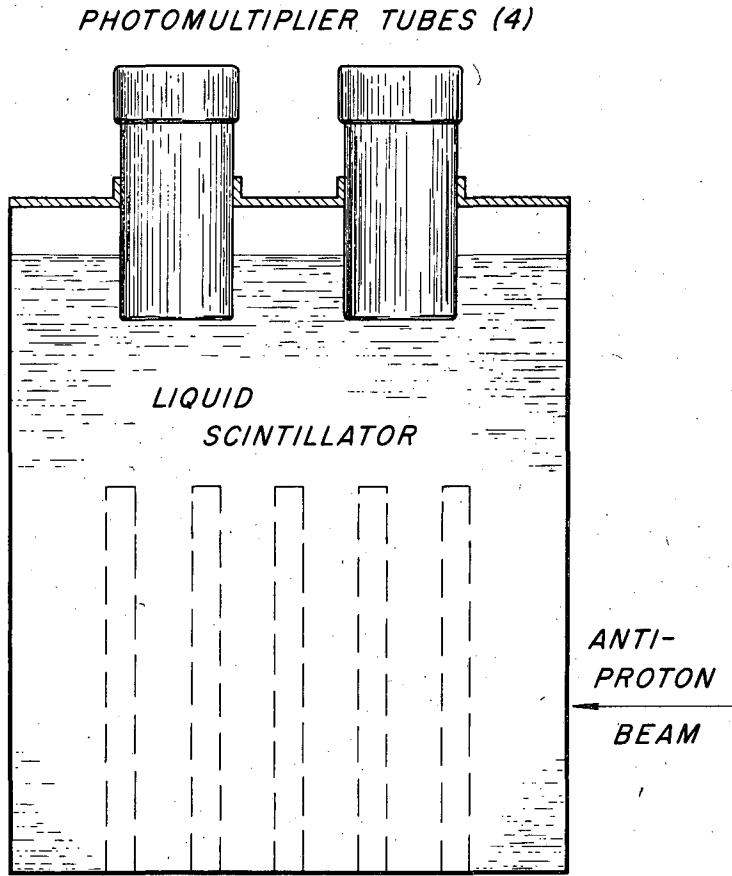


Fig. 6



MU-12625

Fig. 7

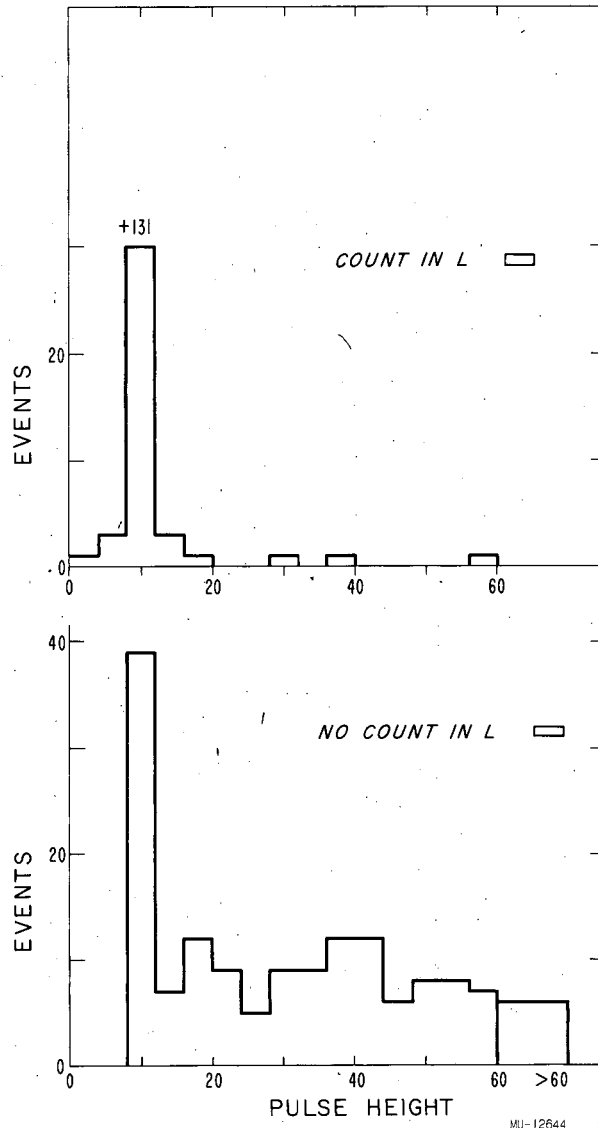
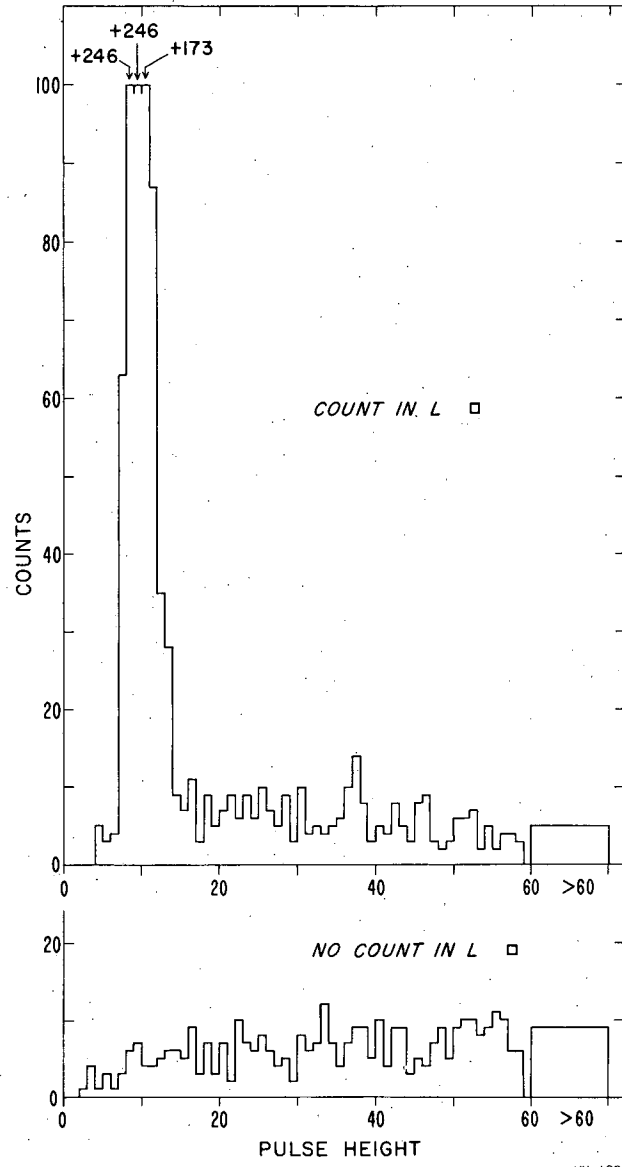


Fig. 8



MU-12835

Fig. 9